ORIGINAL ARTICLE

Journal of
Food Process Engineering

WILEY

Ultrafast extraction of cold brew coffee in a planetary rotating bed reactor: A kinetic study on the pushback effect

Christian von Heynitz[1,2] ⓘ | Kilian Ohlmann[3] | Benedikt Schmieder[1,4] ⓘ | Thomas Hofmann[1,2] ⓘ | Karl Glas[1,2]

[1]Technical University of Munich, Munich, Germany

[2]Chair of Food Chemistry and Molecular Sensory Science, TUM School of Life Sciences, Freising, Germany

[3]Albert Frey AG, Wald, Germany

[4]Biothermodynamics, Freising, Germany

Correspondence
Christian von Heynitz, Chair of Food Chemistry and Molecular Sensory Science, TUM School of Life Sciences, Maximus-von-Imhof Forum 2, 85354 Freising, Germany.
Email: c.heynitz@tum.de

Abstract

Given the rising demand for cold brew coffee, innovative approaches are required to address the present difficulties in its production. This motivates the consideration of the planetary rotating bed reactor (PRBR) as a solid–liquid extraction technology. The PRBR consists of cylindrical mesh chambers that contain the solid phase and move in two superimposed rotations. This motion pattern enhances mass transfer through alternating radial forces: the pushback effect (PBE). To evaluate the utility of the PRBR and the role of PBE, we investigated the kinetics and energy demand of cold brew coffee extraction. For this purpose, we varied rotational speeds and PBE conditions in a 1 L lab-scale reactor. Kinetics was determined by in-line monitoring of electrical conductivity correlated with the eluate's weight-based total dissolved solids and caffeine by high-performance liquid chromatography. Energy consumption was derived from strain gauge torque measurements. Our findings reveal that saturation of the extraction rate with respect to the rotational speed is evident both with and without PBE. However, PBE significantly reduces extraction time by 75% while requiring 60% less mechanical energy. The fastest conditions probed 95% of the maximum extraction yield within 12 s, effectively being >99% faster than static immersion. We believe these findings, along with further procedural advantages, qualify the PRBR as a viable technology for cold brew coffee production.

Practical Applications

The relevance of an economical and sustainable preparation of cold brew coffee extends from the industrial to the gastronomic to the domestic environment. Challenges and limitations relate to process time, particle separation, product and extraction yield, and taste problems due to over-extraction. The planetary rotating bed reactor (PRBR) promises to address all these issues by combining extraction and separation in a simultaneous and ultrafast process. The present study confirms the superiority of PRBR's action mechanisms in terms of rapidity and energetic efficiency for extraction. Due to the excellent scalability of both the design and the physical effect, the PRBR is intended for large-scale production of ready-to-drink products and local

production in coffee shops or private households. By modifying the particle feed, even continuous operation is conceivable. Further applications are, for example, dry-hopping of beer, fast-aging of spirits, and preparation of various liquid foods.

1 | INTRODUCTION

In recent years, cold brew coffee has witnessed a continuous surge in popularity owing to its distinctive flavor profile and perceived sustainability record compared to its hot-brewed counterpart (Technavio, 2022). Cold brew coffee is typically brewed at or below room temperature, resulting in a less acidic and smoother taste (Batali et al., 2022). Despite its growing demand, the industrial, gastronomical, and domestic production of cold brew coffee poses several challenges. These need to be addressed to increase process efficiency while ensuring product quality. This concerns reducing process time, minimizing the need for postextraction filtration, preventing over-extraction (bitter taste), and maximizing the product and extraction yield (EY) (Cordoba et al., 2019; Kwok et al., 2020).

1.1 | Challenges in cold brew extraction

Due to the exclusion of thermal energy input, cold extraction of coffee holds significant sustainability potential. Still, the long process times of the prevalent static immersion methodology, ranging from several hours to days (Pospisil, 2023; Fuller & Rao, 2017), can be uneconomic in industrial settings and impractical in household and coffeehouse production. Besides techno-economic constraints, the long process times entail additional hygienic and sterility requirements (Kwok et al., 2020; Lachenmeier et al., 2021), as well as the risk of over-extraction of certain compounds and therefore, sensory off-flavors (Cordoba et al., 2019; Morresi et al., 2021). The separation of spent coffee grounds after extraction is a further constraining aspect given some coffee-specific conditions (Bühler et al., 2023). The coffee grinding process causes a broad and usually multimodal particle size distribution. A series of diverse filtration technologies is required to match the range of particle diameters spanning many orders of magnitude (<10 μm to >1 mm) (Severini et al., 2016; Severini et al., 2017; Sympatec, 2023). This problem is further intensified by attempts to shorten the extraction time using stirred tank reactors. Although the processing time may be greatly reduced in this way, the shear force-induced abrasion impacts of the stirring blades generate undefined fine particles that further increase the width of the previously mentioned range (Ravisankar et al., 2023). Furthermore, cold brew coffee is typically stronger than conventional filter coffee and exhibits a higher brew ratio (coffee mass to water volume). This increases the filtration effort and decreases the product yield due to liquid residues in the spent coffee grounds. Both affect process profitability.

Various scientific approaches aim to intensify cold brew extraction using physical mechanisms such as laser irradiation or ultrasonic agitation (Zhai et al., 2022; Ziefuß et al., 2022). To our knowledge, none of these methods is currently in product realization or integrated into the production environment. These technologies, involve high acquisition and operating costs, are difficult to integrate, and are limited in their spatial penetration capacity for larger batch volumes. Furthermore, they do not address the filtration problem nor the dehydration of the spent coffee grounds to maximize product yield.

From these considerations, a pressing need for a superior and affordable process technology can be deduced to 1. drastically shorten the process time, 2. offer realistic filtration options, 3. maximize EY, 4. maximize product yield, and 5. avoid over-extraction.

1.2 | The planetary rotating bed reactor

The planetary rotating bed reactor (PRBR) is a cross-sector technology for solid–liquid reactions in the form of a rotating reactor system (Heynitz, 2020). The application focus is on the highly efficient interaction between a fluid and a particulate solid phase, overcoming the limitations of existing reactor systems in terms of small and clogging-prone particles. The PRBR allows for high mass transfer rates in both directions, from liquid to solid (e.g., adsorption) as well as from solid to liquid, like with the present extraction case (Heynitz et al., 2020).

Conventional rotating bed reactors have been known for decades, and they use centrifugal forces to induce a fluid flow (Magosso, 2015). They offer the possibility of compartmentalizing the solid reaction partner during the interaction with its liquid counterpart. However, these systems are subject to the same procedural disadvantages and limitations as conventional fixed-bed reactors (Heynitz et al., 2020). Higher flow rates and differential pressures lead to increasing compaction and hydraulic degradation of the bed and high energy costs for the pumping. Above all, they lack compatibility with small or deformable particles due to blockages or bypass channel formation within the solid cake (clogging).

The PRBR combines the advantages of bed reactors with those of stirred tank reactors. As can be seen from Figure 1, the PRBR consists of at least one cylindrical chamber in which the particulate solid is trapped. This reactor chamber is encased by a filter mesh, whose defined mesh size controls the retention or release depending on the contained particle size. After off-center placement in the vessel containing the liquid reaction phase, the chamber is moved in a pattern of two superimposed rotations. The first rotation takes place around the

principal axis of the vessel and imposes a circular trajectory of the chamber axis in space. The second rotation occurs relative to the first one but in the opposite direction and around the chamber's principal axis. The resulting motion pattern may be compared to the planetary motion of the Earth around the Sun.

Figure 2 shows a 2D top-view projection of the reactor chamber in two different positions. These positions are defined by the respective opposite locations of the virtual reference point P, fixed on the cylindrical chamber wall. P is used for further consideration of the occurring radial accelerations. Its location is described by the angle φ_2 and the angular velocity ω_2 both spatially relative to rotation #1.

Please note that the angular position of P φ_2 is not associated with a specific chamber position due to the two degrees of freedom defined by the two rotations. Given the discrete rotational symmetry

of the chamber positions, the periodic cycle described by φ_2 defines a complete description of the reactor's steady-state motion. The significance of this periodicity can be derived from the resulting radial acceleration $a_r(\varphi_2)$ at P composed by the centrifugal accelerations of the two partial rotations. This radial acceleration changes its direction relative to the chamber during a cycle and gives rise to a sinusoidal course with respect to φ_2 as shown in Figure 3.

Figure 2 contains the geometric and kinematic quantities to unambiguously describe the chamber's motion. From the radius r_1 of the circular path concerning rotation #1 with angular velocity ω_1, as well as the radius r_2 of the chamber corpus, including ω_2 relative to rotation #1, the occurring radial acceleration a_{out} and a_{in} can be calculated as follows:

$$a_{in} = a_r(\varphi_2 = 0) = -r_2(\omega_1 + \omega_2)^2 - \omega_1^2 r_1$$

$$a_{out} = a_r(\varphi_2 = \pi) = -r_2 \cos\left(\frac{\pi(\omega_1 + \omega_2)}{\omega_2}\right)(\omega_1 + \omega_2)^2 - \omega_1^2 r_1 \cos\left(\frac{\pi\omega_1}{\omega_2}\right)$$

On the one hand, the volume forces embodied by the radial accelerations provide a fluid mechanical driving force that initiates a liquid flow through the chambers. On the other hand, the direction reversal of the radial accelerations relative to the chamber, denoted by the change of sign, causes a pushback effect (PBE) on the particles within (Heynitz et al., 2020). PBE prevents particle clogging and homogenizes the particle bed, inhibiting poorly utilized solid fractions. The PBE can be defined as the ratio of the extremal inbound centrifugal acceleration to the extremal outbound counter acceleration at the opposite point $= |a_{in}/a_{out}|$. As mentioned, this is appropriately defined under the condition of a sign change and, therefore, as an absolute value.

The motion pattern that gives the PRBR its effect can be realized by integrating an adapted planetary gear system. In this way, the reactor chambers borne within a corresponding rotating carrier can be brought into a defined rotation and thereby subjected to PBE.
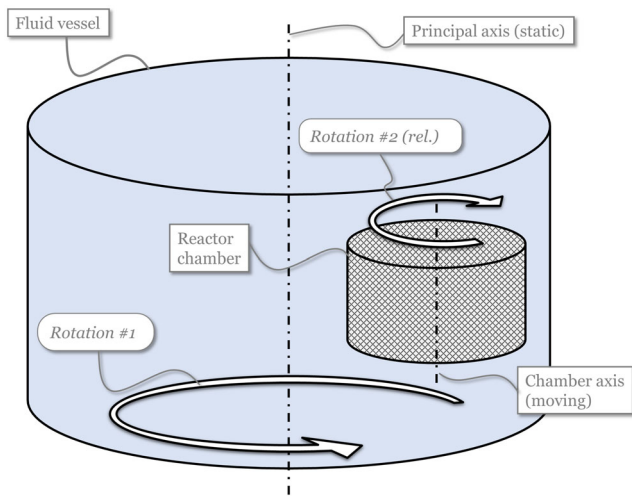
FIGURE 1 Spatial sketch of the reactor chamber comprising the solids and its off-center position within the vessel containing the reaction liquid. The relevant rotational axes with the corresponding spin orientations are indicated.
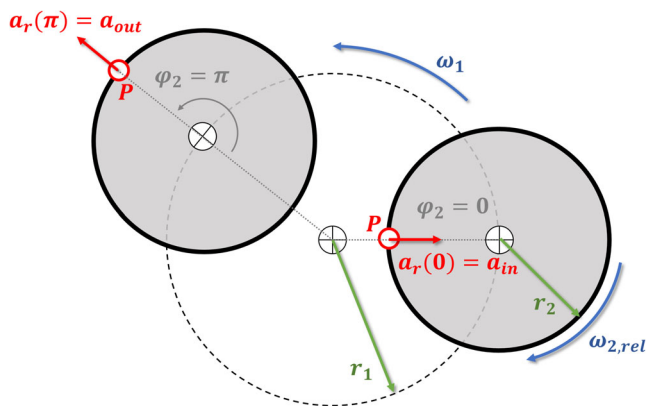
FIGURE 2 2D top-view sketch of the reactor chamber in two different positions regarding rotation #1. The virtual reference point P for observing the radial accelerations is opposite in each case. The relevant rotational velocities ω_i, radii r_i and the vectors of the radial acceleration a_r (a_{in}, a_{out}) are displayed.
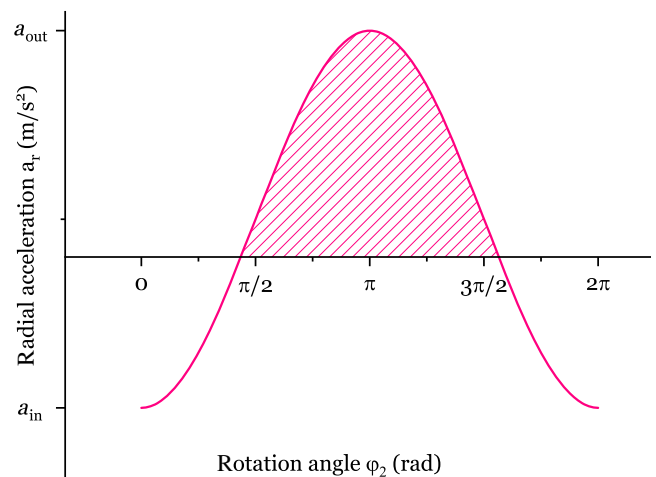
FIGURE 3 Sinusoidal course of the radial acceleration with respect to the relative pose angle φ_2 of the reactor chamber. The zeros indicate the presence of the PBE; their positions (zero G angles) depend on the extent of the PBE and thus the ratio of a_{in} and a_{out}. The enclosed area on the positive ordinate side marks the radial acceleration potential (RAP) (explained in Section 2).

1.3 | The PRBR as extraction platform for cold brew coffee

The growing consumer relevance of cold brew coffee, along with the explained challenges, motivates the consideration of the PRBR as a technological solution. The PRBR promises to significantly speed up the process while minimizing the filtration effort. Furthermore, the flexible choice of mesh size allows small coffee particles to be selectively discharged from the chambers and thus excluded from the intensive mechanical agitation regime (PBE). This mechanism can be employed to avoid sensory over-extraction and intentional dosing of fine particles in the final product. The constant circulation of the ground coffee within the chambers supports a complete and spatially homogeneous dissolution of the components intended for mass transfer. The radial forces acting within the chambers can be exploited to centrifuge out liquid product residues from the spent coffee ground. This dehumidification increases the product yield and reduces the mass of coffee grounds requiring disposal. Therefore, this study aims to validate and deepen the comprehension of the application potentials of the PRBR for cold brew coffee production from kinetic and energetic perspectives, especially with a view to industrial scaling and integration.

2 | MATERIALS AND METHODS

2.1 | Process media

2.1.1 | Coffee

A degassed homogenous batch of fine-ground Brazilian Arabica beans from Kaffee Welt 24 (Wendlingen, Germany) served as processed coffee. We determined the particle size distribution using a laser-diffraction-based HELOS/KR preceded by a RODOS dry disperser (both from Sympatec, Königsbrunn, Germany). As depicted in Figure 4, despite the fine grind, the typical bimodal distribution of coffee is still apparent. The d10 (cumulative size of smallest 10% volume fraction) of 23 μm in accordance with the selected reactor chamber mesh size of 25 μm ensures a moderate ratio of particle retention (agitation) to release (e.g., preventing sensory over-extraction).

2.1.2 | Water

The process fluid was municipal tap water from the city of Freising that contains the following reported (Freisinger Stadtwerke, 2023) mineralization: 93 mg/L of calcium, 26 mg/L of sodium, 3.2 mg/L of potassium, 19 mg/L of nitrate, 40 mg/L of chloride, 41 mg/L sulfate, and 333 mg/L of hydrogen carbonate.

This composition led to a 750 μS/cm withdrawal conductivity at our tapping point. For the process feed, the water temperature was leveled to 20°C using the lab room temperature.
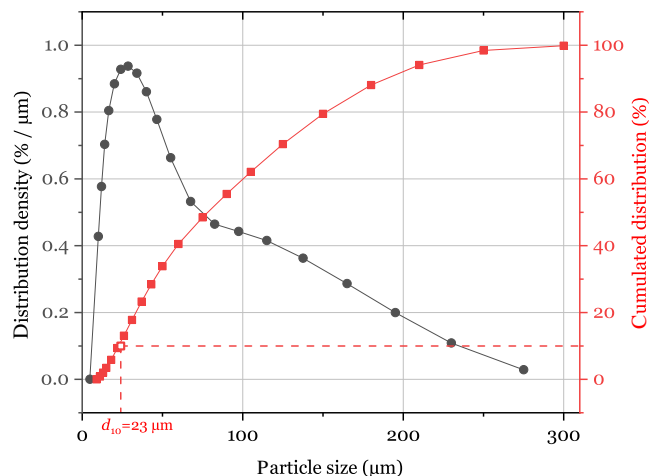
FIGURE 4 Volumetric particle size distribution of the fine ground coffee used for the experiments, obtained by powder laser diffractometry and depicted as cumulative and density function. The scaling is linear to avoid logarithmic distortion of the distribution function.

2.2 | Testing environment

2.2.1 | Lab-scale reactor

The PRBR technology has been implemented in a lab-scale test bench comprising three identical and axisymmetrically arranged reactor chambers, borne within a planetary carrier via their respective planetary shafts (Figure 5a). Each chamber exhibits a diameter of 57 mm, a height of 45 mm, a net fill volume of 100 mL, and a mesh size of 25 μm. Apart from their intended self-rotation relative to the carrier, they are configured to move along a concentric circle with a radius of 36 mm. This corresponds to their respective bearing pattern (Figure 5b).

The superimposed rotation pattern is provided by a double-stage planetary gear set installed at the bottom of the carrier. It comprises a concentrically mounted sun gear, three intermediate gears in mesh with it, and the planetary gears linked to the reactor chambers. The polymer gears all have a modulus of 1, a tooth width of 6 mm, and an effective diameter of 28 mm. This results in a gear ratio of $i = 1$.

The planetary carrier can be borne rotationally in an extraction vessel ($d_i = 140$ mm), whose fluid capacity under the given process totals 1150 mL (Figure 5c). A drive shaft entering through the vessel's top plate drives the planetary carrier, and a drive shaft passing through the bottom plate drives the sun gear. This enables all degrees of freedom of the chamber movement to be mapped within the speed ranges given by the electric drives. Two Oriental BLE2 brushless motors were used as process drives with electronically commutated 3-phase AC supply from a corresponding Oriental BLE2 controller (both Oriental Motor Co., Ltd., Tokyo, Japan).

2.2.2 | Online process measurement

Extraction progress was measured in-line using an ecoLine CR-PVC (JUMO GmbH & Co. KG, Fulda, Germany) two-electrode electrical
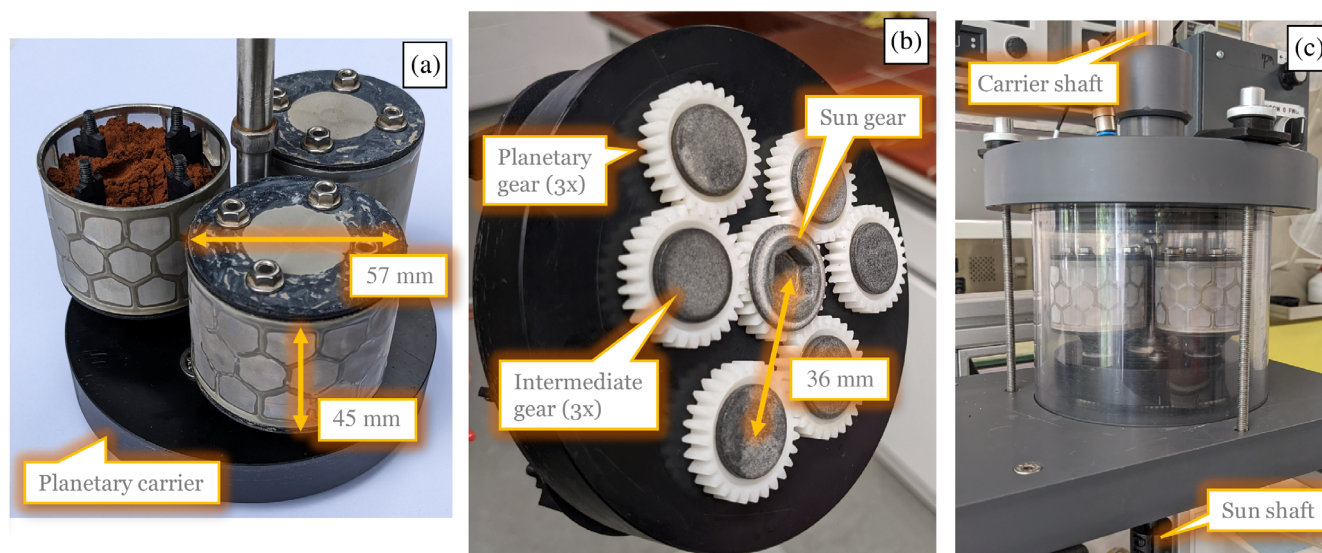
FIGURE 5 PRBR test bench: (a) Meshed reactor chambers with indicated measures, borne in a planetary carrier. (b) Planetary gear drives on the bottom side of the carrier with indicated gear wheels and radius of circle trajectory. (c) Extraction vessel with incoming drive shafts.

conductivity (EC) sensor (cell constant $K = 1.0$), which was integrated into the vessel's bottom plate and connected to an AQUIS 500 CR (JUMO GmbH & Co. KG, Fulda, Germany) data transmitter. The transmitter also accesses the analog temperature signal of a resistance thermometer sensor (Pt100) in the bottom plate to allow for thermal conductivity correction. We are aware that EC addresses substances with an external electrical net charge and thus does not directly cover the complete entity of dissolved substances in coffee. However, the entire test campaign was carried out with the same coffee raw material, water matrix, temperature, and extraction technology. Thus, we consider the EC as sufficiently representative of the process kinetics and to identify a reliable correlation with the total dissolved solids (TDSs)/caffeine concentration and the entire solute entity. Since the present study concerns an initial proof-of-concept focusing on kinetic comparisons, commonly encountered parameters, such as trigonelline and chlorogenic acids, etc., have not been analyzed.

The torque required to determine the mechanical energy demand was measured by load cells HX711 (Funduino GmbH, Nordhorn, Germany), which receive the reaction force of the process torque via a defined lever of the motor modules mounted in rotary bearings for this purpose. The analog force value of the cell was registered with an Arduino Uno board (Funduino GmbH, Nordhorn, Germany), converted to a torque based on lever arm dimensions, and passed on accordingly. On-site visualization and data storage were carried out using an Ecograph T RSG 235 (Endress & Hauser GmbH & Co. KG, Maulburg, Germany), which processed the incoming analog signals.

2.2.3 | Peripheral devices

Before every experiment, the reaction vessel was fed with process water using a Hei-FLOW Ultimate 600 (Heidolph GmbH, Schwabach,

Germany) peristaltic pump, maintaining a flow rate of 50 mL/s with an intended pause as soon as the water leveled with the upper side of the reactor chambers to ensure comprehensive flooding and therefor drive out potential air residues. For weighing the ground process coffee, we used a 500 M-2000C (PRECISA Gravimetrics AG, Dietikon, Switzerland) balance. For cleaning, the reactor chambers and their filter mesh were exposed to an ultrasonic bath Emmi 20 (EMAG AG, Mörfelden, Germany) with a surfactant dissolved in deionized water.

2.3 | Offline analytics

During the extraction experiments, samples with a volume of 3 mL each were drawn into a 5-mL syringe via a Luer-compatible valve in the vessel jacket and cleared of dispersed particles with a 0.20-μm syringe filter Chromafil PET-20/15 MS (Macherey-Nagel GmbH & Co. KG, Germany).

2.3.1 | Total dissolved solids and extraction yield

The TDS of the samples was determined by difference weighing compliant with DIN 10775 (Deutsches Institut für Normung e.V., 2016) using a BP 221 S (Sartorius AG, Göttingen, Germany) analytical balance. A weighted fluid sample was evaporated to dryness in a preweighed aluminum dish. The dish was placed in a 2738 (Köttermann GmbH, Uetze, Germany) compartment dryer at 80°C for 5 h. After cooling in a desiccator, the dish was reweighed. The TDS was calculated by subtracting the empty evaporating dish's weight from the dish's weight plus the dried residue. The TDS results were expressed in mass percent (%). The TDS in combination with the known batch mass of initial process water m_{fluid} as well as the mass of coffee m_{coffee}

used per batch allows the determination of the EY (%), considering the TDS of the tap water TDS_0:

$$EY = \frac{(TDS - TDS_0) \times m_{fluid}}{m_{coffee}}$$

2.3.2 | High-performance liquid chromatography analysis of caffeine

The caffeine content was determined at a wavelength of $\lambda = 272$ nm by high-performance liquid chromatography (HPLC) on a 1290 Infinity LC (Agilent Technologies, Inc., USA) equipped with an ultraviolet–visible detector and the reverse phase column VDSpher PUR C18-E (150 mm × 4.6 mm, 5 μm; VDS optilab Chromatographie Technik GmbH, Germany). The undiluted samples were stored at 9°C. For the analysis, the method described in Schmieder et al. (2023) was utilized: Eluent A consisted of HPLC-water (≥99.9%, HiPerSolv Chromanorm) with 0.5% formic acid (≥98%, AnalaR Normapur) and eluent B of methanol (≥99.9%, HiPerSolv Chromanorm Reag. Ph. Eur.) with 0.5% formic acid (≥98%, AnalaR Normapur). At a constant flow rate of 1.2 mL/min, the following gradient method was used for 10 μL injected sample volume: 2% B (0–1.2 min), 20% B (2.5 min), 40% B (13 min), 95% B (14.5–15 min), 2% B (15.5–21 min). The chemicals were acquired from VWR Chemicals GmbH (Germany), and the caffeine analytic standard (≥99.0%, C0750) from Sigma Aldrich (Germany) was used for the calibration.

2.4 | Technical, physical, and economic reference metrics

This investigation requires appropriate reference quantities to compare the process times with and without PBE. Since the PBE motion comprises two rotations, it lacks a unique reference speed for comparison with the self-rotation without PBE, described by solely one speed. Thus, we defined three domains from different points of view.

The technical domain considers the speed of the electric motor n_M and represents an application-oriented engineering perspective. It relates to the availability and rpm-torque characteristics of drive systems and rotating components' work safety and maintenance intensity.

The physical domain considers the (fluid-) mechanical effect caused by the rotations. To express the chamber's percolation intensity by only one parameter, we have introduced the radial acceleration potential (RAP) given by the area under the positive part of the acceleration curve (Figure 3). For PBE setups hold,

$$RAP = \int_{\phi_1^{zeroG}}^{\phi_2^{zeroG}} a_r(\varphi) d\varphi$$

with ϕ_i^{zeroG} being the axis intersection point, characterized by radial zero gravity. For no PBE, this reduces to $RAP = 2\pi a_r = 2\pi r_2 \omega_2^2$. The RAP can, thus, be comprehended as the intensity of the fluid conveying (pumping) angular phase as of a flow rate equivalent.

The sustainability domain combines both economic and ecological perspectives by considering the processual demand for mechanical energy. The calculations are based on determining the mechanical power consumption delivered by the drive shafts. Due to the reactors, steady-state operation applies $E_P = T\omega_M t_P$ with T denoting the shaft torque, ω_M the engine torque, and t_P a process time descriptor.

2.5 | Experimental design

The experimental design considers statistical robustness, a parameter space that addresses the scientific question while respecting food and drinking water use. Following the coarse scanning carried out upfront, seven speed levels each were defined with and without PBE and mapped in a randomized experimental schedule. The center and edge speeds were determined twice, resulting in 20 single experiments (Table 1).

2.6 | Data processing and kinetic modeling

All data analysis steps, including import, processing, regression, parameter derivation, and visualization, were performed using OriginPro (OriginLab Corporation, Version 2023b). The Weibull cumulative distribution function was the only mathematical description adequate to represent the encountered extraction kinetics. This is not surprising, as the same function has already been shown to be suitable for the kinetics of coffee extraction (Wang & Lim, 2021). Regarding the EC measured online, the equation is:

$$\kappa(t) = \kappa_{max} \left(1 - \exp\left(-k^d (t - \Delta t)^d \right) \right)$$

κ_{max} indicates the equilibrium value, k and d kinetic parameters, and Δt a shift along the time axis to allow for curve fitting

TABLE 1 Parameter overview of the performed experiments containing relevant speeds (rpm) and derived radial acceleration potential (RAP), categorized by pushback-effect (PBE).

| rpm level | No PBE | | PBE | |
| | Shaft/chamber | | Shaft/carrier | |
	rpm	RAP (−)	rpm	RAP (−)
#1[a]	600	64.5	316	7.2
#2	700	87.7	394	11.2
#3	800	114.6	473	16.1
#4[a]	900	145	552	28.7
#5	1000	179.1	710	36.3
#6	1100	216.7	789	44.8
#7[a]	1200	257.9	947	64.5

Abbreviations: PBE, pushback effect; RAP, radial acceleration potential.
[a]Double determination.

independent from starting time. Given the linear correlation between TDS/caffeine and EC (illustrated in the results section), the Weibull function can be jointly applied for all three quantities (TDS, caffeine, and EC). The common process time t_{95} can, therefore, be derived as:

$$t_{95}(k,d) = \frac{1}{k}\left[\ln\left(\frac{1}{1-\psi}\right)\right]^{\frac{1}{d}} \text{with } \psi = \frac{\kappa}{\kappa_{\max}} = 0.95$$

This t_{95} indicates the period required to reach 95% of the equilibrium value and marks the principal benchmark for this study.

All underlying curve-fitting operations were conducted using the Levenberg–Marquardt algorithm. We implemented the Gaussian error propagation to apply the parameter standard errors ε_i within the curve fitting to the process time t_{95}:

$$\varepsilon_t = \sqrt{\left(\frac{\partial t(k,d)}{\partial k}\varepsilon_k\right)^2 + \left(\frac{\partial t(k,d)}{\partial d}\varepsilon_d\right)^2}$$

$$= \sqrt[d]{\ln^2\left(\frac{1}{1-\psi}\right)}\sqrt{\frac{\varepsilon_k^2}{k^4} + \frac{\log^2\left(\ln\left(\frac{1}{1-\psi}\right)\right)}{d^4}\varepsilon_d^2}$$

3 | RESULTS AND DISCUSSION

3.1 | Correlation between TDS/caffeine and electrical conductivity

Essential to the testimony of the study is the synthesis of the real-time capable EC measurement with the process relevance of TDS and caffeine concentration. Identified as linear, both relationships are illustrated in Figure 6, along with the corresponding regression. Since the faster experiments with high rpm led to a very steep increase in conductivity, the first seconds are unsuitable for taking samples with a reliable time-stamp. Therefore, more data points are available in the

higher EC range than in the lower one. However, the correctness of the correlation is validated by the consistency with the tap water EC/TDS marked by an asterisk. Randomization of sampling ensures calibration reliability across different speed levels and PBE configurations.

3.2 | Time course of electrical conductivity

We consider the EC over time distinguished by PBE mode (Figure 7). The curves are referenced to the RAP. The ordering adjusts according to RAP, and a PBE-mode-specific curvature is apparent. Selected data points of the acceleration phase have been masked. The time axis scaling is square root scaled for more convenient graphical delimitation. A visual assessment of the data suggests a reasonable choice of rpm/RAP range, as saturation of extraction rate with respect to RAP can be observed. Given the difficulty of defining an exact start time for each curve, a detailed quantitative evaluation of the extractions' kinetic requires curve fitting analysis, employed in the further course. However, it is already evident that PBE leads to faster extraction and shorter minimum process times.

The independence of the equilibrium values from the PBE mode was proven using a two-sample minor t-test. After the Shapiro–Wilk test for both data sets (no PBE and PBE) proved the presence of a normal distribution at a significance level of 0.05, the proof of independence also followed at a significance level of 0.05 and a t-value of 0.41693 (Figure 8). Therefore, the minor existing variations are assumed as the result of fluctuating tap water conditions (e.g., mineral interactions).

### 3.3 | Characterization of the finished cold brew

Based on the previous results, the average final TDS is 1.20%, which is reduced to a net 1.09% after correction for the mineralization of
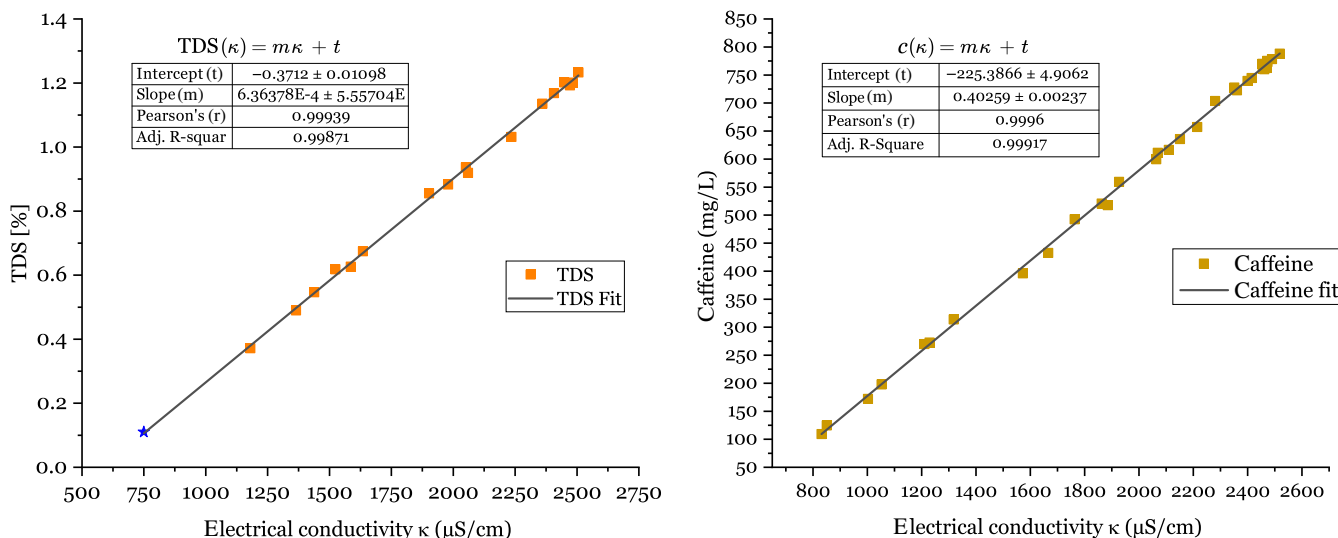
FIGURE 6 Plot of linear correlation between gravimetrically determined TDS value and HPLC-based caffeine concentration of each randomized drawn sample and the respective conductivity levels.
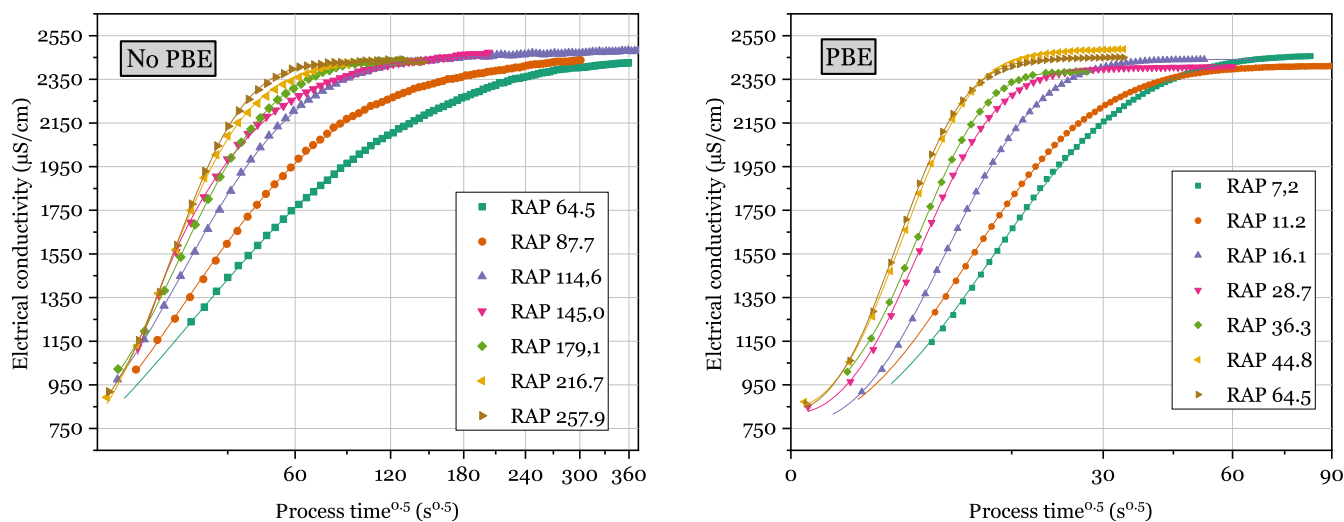
FIGURE 7 Temporal evolution of electrical conductivity across all experimental setups (excl. doubles), considered separately without PBE (left) and with PBE (right), and displayed with a square root time axis.
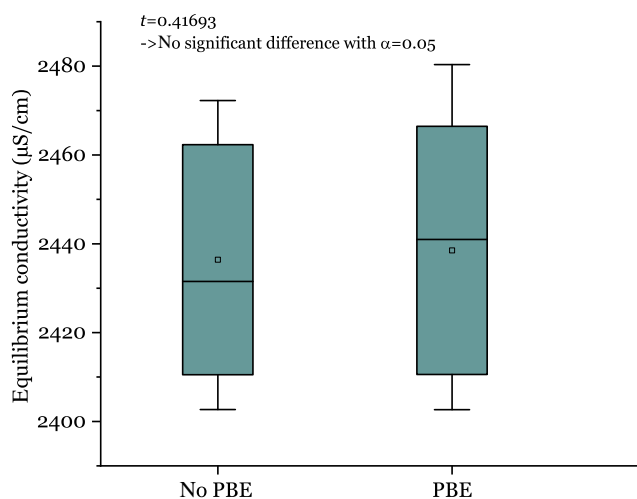
FIGURE 8 Comparison of the equilibrium values of electrical conductivity obtained by curve fitting. After the respective proof of a normal distribution, the t-test confirms the final extraction result's significant (0.05) independence from the reactor settings. Indicated are mean (dot), median (line), standard deviation (box), and 5–95 confidence intervals (whisker).

the tap water. In conjunction with the batch quantity of ground coffee of 60 g and a water volume of 1150 mL, a decent EY of 20.9% is achieved. This is accompanied by an average caffeine content of 770 mg/L. Despite the test bench optimization for scientific purposes, both values are familiar figures for industrially produced cold brew coffee (Pan et al., 2023; Washington, 2016) and thus embody a realistic case study.

3.4 | Torque characteristics

The quantification of process energy is based on the measurement of the drivetrain torques and the derived mechanical power. Figure 9

shows the curves of the shaft torque for both modes in the relevant speed range. As expected, both characteristic curves follow a parabolic course by the nature of a turbulent flow and were, thus, fitted by $y = ax^2 + c$. It is plausible that the PBE torque increases more steeply with rpm due to the more complex and friction-prone fluid mechanical conditions. The difference in torque base level (rpm ~ 0) is not technology-related and arises from friction with power train shaft sealing and bearing. In contrast to the frictions mentioned above, this is rigid body friction with torque not dependent on rpm. This proportion was eliminated for further processing by exclusively considering the coefficient a of the fitting formula. As mentioned in the method section, a direct comparison of the curves between noPBE and PBE yields no reliable information since the speeds are not comparable without the context of the processing time and, as a result, derived energy. The mechanical power for the further process energy considerations was derived from the torque (fitted), and the associated speed is displayed in Figure 9.

3.5 | Process time with respect to the reference metric

Figure 10 presents the PBE-classified process times t_{95} with respect to the technical domain (left) and the physical domain (right). Both perspectives confirm the superiority of PBE since all process times with PBE are lower than those without PBE. A considerable improvement can be seen regarding kinetic saturation in the asymptotic range. Saturation is meant as a stagnant extraction rate with increasing speed. For example, these saturation values differ by a factor of four with respect to t_{95} and, thus, a reduction of 75% of the process time. For the mode without PBE, this can be explained by increasing centrifugal compression of the particle bed and, thus, poorer flow hydraulics. In contrast, the constant mobility of the coffee particles in the PBE mode suggests a grain diffusion limitation at the single particle level. It can be deduced that PBE better exploits the physical
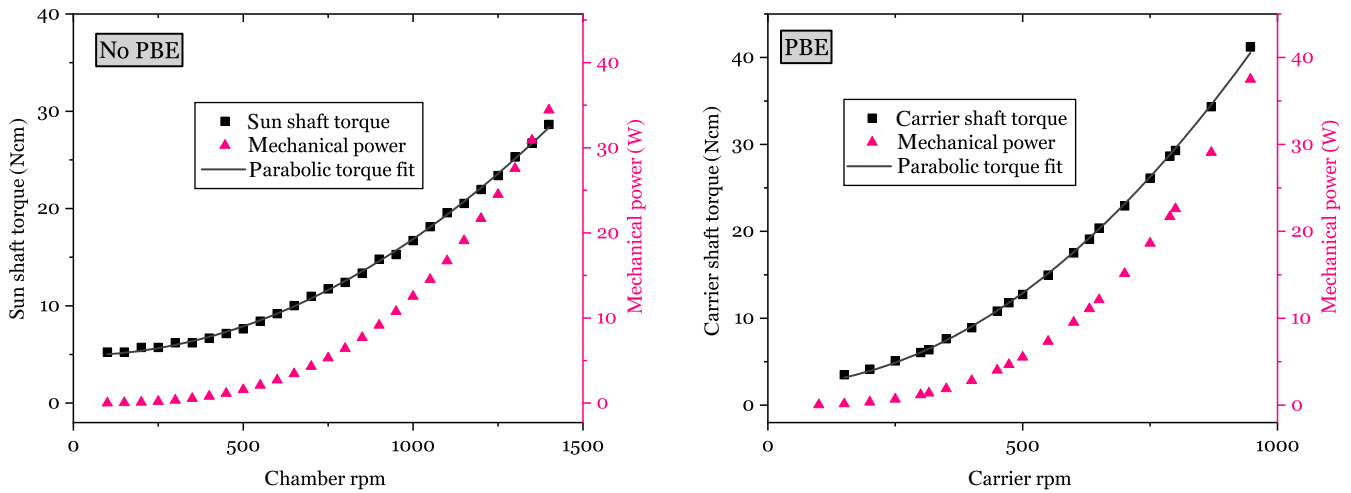
FIGURE 9 Torque and mechanical power curve plotted against respective drive rpm (no PBE left, PBE right). The mechanical power is derived from the torque corrected for nontechnological frictional effects.
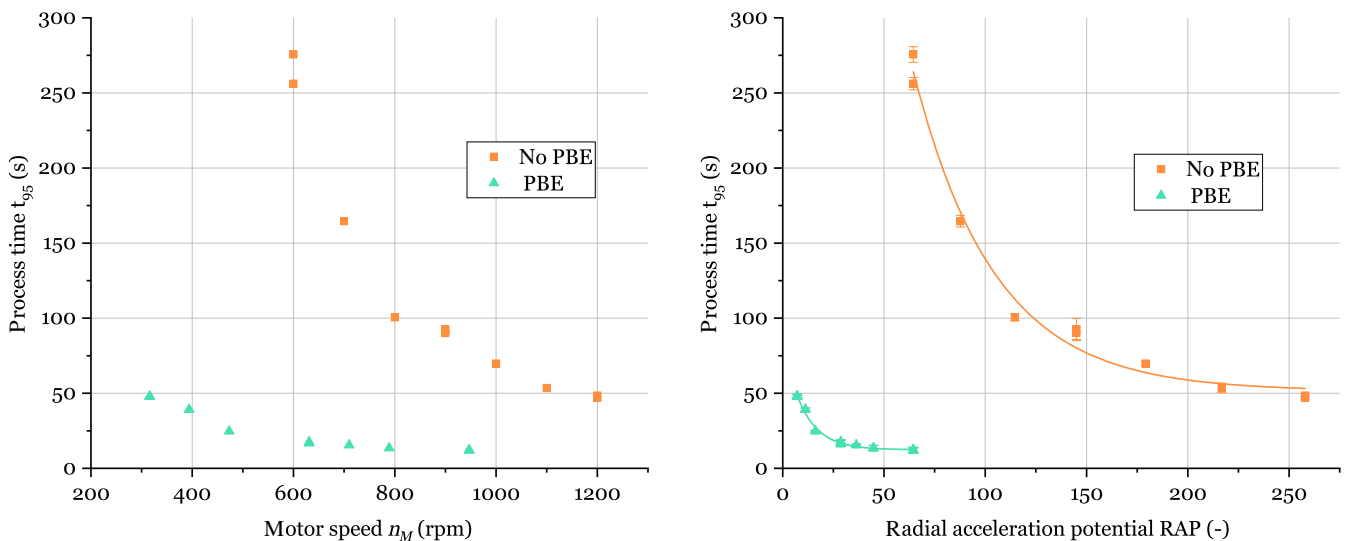
FIGURE 10 Process times t_{95} from a technical and physical perspective with corresponding motor speed (left) and radial acceleration potential (RAP) (right). The RAP-dependent graph (right) includes the propagated standard errors from the kinetic curve fitting as well as a fitting of the course itself.

possibilities of maximum extraction (film diffusion) since there is no macroscopic limitation due to the particle bed and its hydraulics. Because the two plots only differ in the reference metric, the propagated standard errors are solely displayed in the RAP metric. In addition, a pragmatic fit using the function $y = A \times \exp\left(-\frac{x}{t1}\right) + y0$ is added in this one. Since the PRBR technology was investigated experimentally for the first time in the present work, this approach function is the outcome of an engineering intuition. However, it smooths the data for further calculation of the process energy. The quality parameters of the Weibull curve fitting the extraction are summarized in Table 2.

The remaining perspective is sustainability in terms of energy demand concerning the mechanical power input. This domain bundles the results of the extraction kinetics with those of the torque

measurement and is demonstrated in Figure 11. The results complete previous interpretations of the procedural superiority of PBE. They prove the higher flow forces and torques that PBE entails to be a sensible investment since the effect of time savings outweighs the power requirement. For instance, the previously highlighted process time reduction of 75% is accompanied by mechanical energy input reduction of 60%. Also, in this domain, the Pareto front of noPBE runs entirely in the inferior range compared to PBE. Because the determination of the process energy relies on the process time, both axes are mathematically coupled. As introduced before, the results are the outcome of data smoothing by curve fitting. We note that the calculated values of process energy are suitable only for a relative comparison among themselves. A universally applicable quantification of energy requirement is not possible, as it heavily depends on the termination

TABLE 2 Weibull fitting qualities Chi-square and adjusted R^2 of time courses and process time t_{95} with respect to radial acceleration potential (RAP) and categorized by the pushback effect (PBE).

rp m level	No PBE				PBE			
	RAP (−)	t_{95} (s)	Chi-square	Adj. R^2	RAP (−)	t_{95} (s)	Chi-square	Adj. R^2
#1[a]	64.5	256.1	21.13	0.99975	7.2	48.00	12.19	0.9999
#1[a]	64.5	275.6	19.75	0.99977	7.2	47.75	5.30	0.99994
#2	87.7	164.6	51.30	0.99951	11.2	39.15	2.97	0.99996
#3	114.6	100.6	47.47	0.99942	16.1	24.67	3.89	0.99998
#4[a]	145	90.1	85.92	0.99913	28.7	17.46	31.81	0.99978
#4[a]	145	92.4	51.33	0.99933	28.7	16.68	16.46	0.99982
#5	179.1	69.8	18.19	0.99987	36.3	15.41	7.7	0.99996
#6	216.7	47.0	46.22	0.99976	44.8	13.49	53.35	0.99973
#7[a]	257.9	53.5	119.15	0.99929	64.5	12.26	48.96	0.99973
#7[a]	257.9	48.5	26.53	0.99979	64.5	12.00	42.32	0.99977

Abbreviations: PBE, pushback effect; RAP, radial acceleration potential.
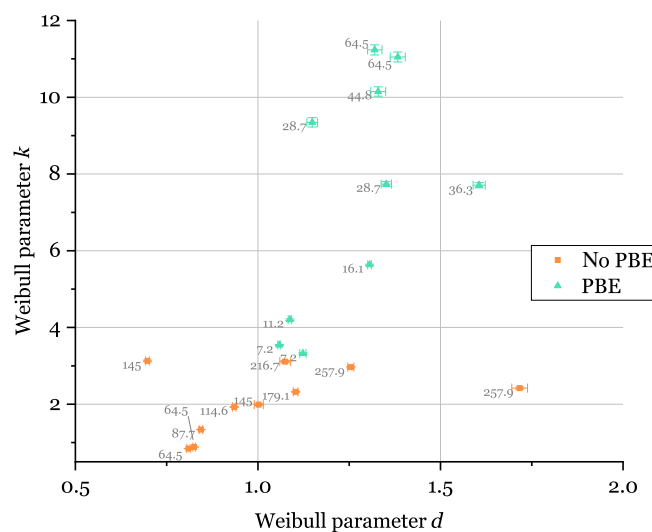[a]Duplicate determinations are marked by cross.
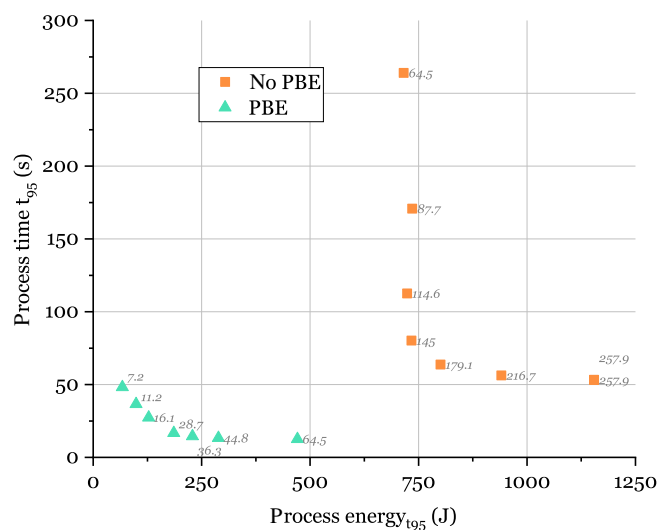
FIGURE 11 Relationship between process time and energy input based on mechanical power and that same process time. All underlying data were fit to the smoothing in favor and to avoid amplified error propagation.

FIGURE 12 Mutual dependence of the two fitted Weibull kinetics parameters d and k for the respective PBE regimes. The apparent and nonrandomly distributed correlation confirms the validity of the fitting function.

3.6 | Fitting parameter behavior

The Weibull function used for fitting the extraction course contains two kinetic parameters d and k. Because within a given PBE mode, only one process parameter was varied (rotational speed), a closer look at the relation between d and k is sensible. This relationship is plotted

criterion of the extraction process. In this case, the calculation was based on the process times t_{95} as defined in the methods section. Therefore, no liquid volume-specific energy consumptions were derived.

in Figure 12, along with the fitting standard error and the corresponding RAP. Despite the outlier, a significant structure is visible for both PBE modes. The setups without PBE show a significantly larger parameter dependence of d than with PBE. This dependence goes hand in hand with the RAP, whereas for PBE, this relation is much less significant. In summary, the presence of unique and nonrandom patterns confirms the validity of the Weibull cumulative distribution as an approach function and attributes the excellent adjusted error squares (adj. R^2). We note that parameter d as a power quantity is susceptible to adjustments at the cutoff of the acceleration phase. For this study, however, this is not problematic because the interactive changes in d and k do not lead to any significant change in the process time.

4 | CONCLUSIONS

The growing demand for cold brew coffee is still accompanied by numerous challenges regarding production technology. Therefore, we investigated the performance of the PRBR for cold brew coffee extraction. Over the whole investigated speed range, the PBE as the key mechanism shortened process time while reducing energy consumption. The full-range superiority was also shown when comparing process time based on engine speed as a technical reference and RAP as a physical reference.

Both modes with and without PBE showed a saturation of process time with increasing rotational speed. PBE decreased the shortest possible process time t_{95} by 75% while requiring 60% less mechanical energy. The absolute timespan of 12 s to reach 95% of the maximum EY of 20.9% is highly competitive with other extraction technologies. The PRBR minimizes filtration effort by compartmentalizing the ground coffee during extraction. Since this option is usually only available in static immersion (e.g., bags), the latter is the most appropriate reference technology. Compared with static immersion, process time was reduced by over 99%. The representative calculation of the process time was made possible by the linear relationship between EC and caffeine and TDS, respectively.

Along with other benefits, some of which still need to be proven and quantified, the PRBR is a promising technology for process integration. The associated PBE suggests being a powerful tool for process intensification. Further investigations are planned and concern the scale-up in the radial and axial directions, the adjustment of the mesh sizes, the spent coffee dehydration, as well as the loading quantity of the chambers.

CONFLICT OF INTEREST STATEMENT

Mr. Christian von Heynitz is the inventor of patent #EP3669976B1 issued to the Technical University of Munich, including the rights to the federal German employee invention law.

DATA AVAILABILITY STATEMENT

The data that support the findings of this study are available from the corresponding author upon reasonable request.

AUTHOR CONTRIBUTION STATEMENT

Christian von Heynitz: Conceptualization; project administration; visualization; writing—original draft. **Kilian Ohlmann**: Resources; investigation; methodology. **Benedikt Schmieder**: Data curation; process analytics. **Thomas Hofmann**: Funding acquisition; writing—review and editing. **Karl Glas**: Supervision; formal analysis; validation.

ORCID

Christian von Heynitz ⬤ https://orcid.org/0000-0002-8049-114X
Benedikt Schmieder ⬤ https://orcid.org/0009-0001-3134-7926
Thomas Hofmann ⬤ https://orcid.org/0000-0003-4057-7165

REFERENCES

Batali, M. E., Lim, L. X., Liang, J., Yeager, S. E., Thompson, A. N., Han, J., … Guinard, J.-X. (2022). Sensory analysis of full immersion coffee: Cold brew is more floral, and less bitter, sour, and rubbery than hot brew. *Foods*, *11*(16), 2440. https://doi.org/10.3390/foods11162440

Bühler, B., Foik, S.-M., Bäuerle, T., Schwarz, S., Winkler, G., & Lachenmeier, D. W. (2023). Cold-brew coffee: Investigation on consumer expectation and trade conception; [cold-brew-Kaffee Untersuchung zu Konsumentenerwartung und Verkehrsauffassung]. *Deutsche Lebensmittel-Rundschau*, *119*(1), 6–10. https://doi.org/10.5281/zenodo.7547316

Cordoba, N., Pataquiva, L., Osorio, C., Moreno, F. L. M., & Ruiz, R. Y. (2019). Effect of grinding, extraction time and type of coffee on the physicochemical and flavour characteristics of cold brew coffee. *Scientific Reports*, *9*(1), 8440. https://doi.org/10.1038/s41598-019-44886-w

Deutsches Institut für Normung e.V. (2016). *Analysis of coffee and coffee products—Determination of water-soluble extract—Method for roasted coffee*. (norm, DIN 10775). Berlin: Beuth Verlag GmbH: Beuth Verlag GmbH.

Freisinger Stadtwerke. (2023). Trinkwasseranalyse der Stadt Freising für 2023. Freising. https://www.freisinger-stadtwerke.de/de/Administration/Auszeichnungen-Referenzierter-Content/Linke-Seite/Trinkwasseranalyse-2023-klein.pdf

Fuller, M., & Rao, N. Z. (2017). The effect of time, roasting temperature, and grind size on caffeine and chlorogenic acid concentrations in cold brew coffee. *Scientific Reports*, *7*(1), 17979. https://doi.org/10.1038/s41598-017-18247-4

Heynitz, C. v. (2020). Technical University of Munich EP 3 669 976 B1. *Deutschland*.

Heynitz, C. v., Stecker, M., Hofmann, T., & Glas, K. (2020). A novel dry hopping technology: Kinematic modelling of a planetary rotating bed reactor. *BrewingScience*, *73*(3), 68–76. https://doi.org/10.23763/BrSc20-09heynitz

Kwok, R., Lee Wee Ting, K., Schwarz, S., Claassen, L., & Lachenmeier, D. W. (2020). Current challenges of cold brew coffee—Roasting, extraction, flavor profile, contamination, and food safety. *Challenges*, *11*(2), 26. https://doi.org/10.3390/challe11020026

Lachenmeier, D. W., Noack, D., Röhnisch, J., & Seren, H. Y. (2021). Cold brew coffee—A microbial hazard? *Advance Online Publication*, *193*, 32–33. https://doi.org/10.5281/zenodo.4575473

Magosso, M. (2015). *Investigation of the Spinchem® rotating bed reactor: Internally and externally mass transfer limited reactions (Tesi di Laurea Magistrale)*. Università Degli Studi Di Padova.

Morresi, A. M., Truglio, K., Specchio, J., & Kerrihard, A. L. (2021). Effects of grind size and brew time upon sensory traits, consumer likability and antioxidant activity of Arabica cold brew. *International Journal of Food Science & Technology*, *56*(4), 1929–1936. https://doi.org/10.1111/ijfs.14824

Pan, L., Xiao, Y., Jiang, F., Jiang, T., Zhu, J., Tang, W., … Yu, L. (2023). Comparison of haracterization of cold brew and hot brew coffee prepared at various roasting degrees. *Journal of Food Processing and Preservation*, *2023*, 1–15.

Pospisil, A. (2023). *What is the future of cold brew coffee?* https://europeancoffeetrip.com/cold-brew-coffee-future/

Ravisankar, V., Wu, J., Bhargava, S., & Parthasarathy, R. (2023). Studying particle attrition in a solid-liquid agitated vessel using focused beam reflectance measurement (FBRM). *Chemical Engineering and*

Processing—Process Intensification, 183, 109256. https://doi.org/10.1016/j.cep.2022.109256

Schmieder, B. K. L., Pannusch, V. B., Vannieuwenhuyse, L., Briesen, H., & Minceva, M. (2023). Influence of flow rate, particle size, and temperature on espresso extraction kinetics. *Foods, 12*(15), 2871. https://doi.org/10.3390/foods12152871

Severini, C., Derossi, A., Fiore, A. G., De Pilli, T., Alessandrino, O., & Del Mastro, A. (2016). How the variance of some extraction variables may affect the quality of espresso coffees served in coffee shops. *Journal of the Science of Food and Agriculture, 96*(9), 3023–3031. https://doi.org/10.1002/jsfa.7472

Severini, C., Derossi, A., Ricci, I., Fiore, A. G., & Caporizzi, R. (2017). How much caffeine in coffee cup? Effects of processing operations, extraction methods and variables. In J. N. Latosinska & M. Latosinska (Eds.), *The question of caffeine.* InTech. https://doi.org/10.5772/intechopen.69002

Sympatec. (2023, May 17). *Coffee particle size and shape analysis*. https://www.sympatec.com/en/applications/coffee-particle-size-analysis/.

Technavio. (2022). *Cold brew coffee market to record USD 1.37 Bn growth—Driven by increasing popularity of instant coffee among millennials and product launches*. https://www.prnewswire.com/news-releases/cold-brew-coffee-market-to-record-usd-1-37-bn-growth-driven-by-increasing-popularity-of-instant-coffee-among-millennials-and-product-launches-301605228.html.

Wang, X., & Lim, L.-T. (2021). Modeling study of coffee extraction at different temperature and grind size conditions to better understand the cold and hot brewing process. *Journal of Food Process Engineering, 44*(8). https://doi.org/10.1111/jfpe.13748

Washington, S. (2016). The amount of total dissolved solids in coffee made by 6 different brewing methods. *Cantaurus, 2016*(24).

Zhai, X., Yang, M., Zhang, J., Zhang, L., Tian, Y., Li, C., ... Abd El-Aty, A. M. (2022). Feasibility of ultrasound-assisted extraction for accelerated cold brew coffee processing: Characterization and comparison with conventional brewing methods. *Frontiers in Nutrition, 9*, 849811. https://doi.org/10.3389/fnut.2022.849811

Ziefuß, A. R., Hupfeld, T., Meckelmann, S. W., Meyer, M., Schmitz, O. J., Kaziur-Cegla, W., ... Barcikowski, S. (2022). Ultrafast cold-brewing of coffee by picosecond-pulsed laser extraction. *npj Science of Food, 6*(1), 19. https://doi.org/10.1038/s41538-022-00134-6